

Optoelectronic response calculations in the framework of $\mathbf{k} \cdot \mathbf{p}$ coupled to Non-equilibrium Green's functions for 1D systems in the ballistic limit

Andrei Buin,¹ Amit Verma,² and Simarjeet Saini¹

¹*Department of Electrical and Computer Engineering, University of Waterloo,
Waterloo, Ontario N2L 3G1, Canada*

²*Department of Electrical Engineering and Computer Science,
Texas A&M University Kingsville, Kingsville, Texas 78363,
USA*

We present theory of the carrier-optical interaction in 1D systems based on the nonequilibrium Greens function formalism in the 4×4 $\mathbf{k} \cdot \mathbf{p}$ model. As a representative parameters we chose the GaAs. Although theory is presented in 4×4 kp many subbands, results and discussion section is based on the simplified model such as 2×2 kp model (two transverse modes). Even though 2×2 kp model is simple enough it shows many phenomena that have not been seen before. We focus mainly on the ballistic extraction of photogenerated free carriers at the radiative limit which is described by the self-energy term derived in dipole approximation and solved in self-consistent manner with Keldysh quantum kinetic equations. Any relaxation or non-radiative recombination mechanisms as well as excitonic features are neglected. Effect of non-locality of electron-photon self energy term is considered and discussed. Spontaneous emission is also considered and shown to be small in short devices under medium bias conditions. Electron and hole spatial current oscillations are seen and discussed. It is shown that neglecting off-diagonal correlation in the band index not only produces quantitatively wrong results but it also alters the qualitative picture. All simulations are done in the full-rank approximation, with all spatial and band correlation effects are kept intact. This allows us to study not only quantitative effects but also qualitative behaviour.

PACS numbers: 85.60.Gz, 85.35.Ds, 73.50.Pz, 85.35.Be, 85.30.De

I. INTRODUCTION

The past several years has seen a growing interest in nanowires (NWs) such as SiNWs^{1,2}, GeNWs³, and GaAsNWs because of their excellent optoelectronic properties⁴. As few examples, recent experimental work⁵ on the photocurrent response of freely suspended single 140 nm GaAsNWs has shown current as high as ~ 0.45 nA for a titanium:sapphire laser light intensity of 100 W/cm^2 . Experimental work on the effect of strain on GaAsNWs, approximately 80 nm in diameter⁶, and theoretical work on much smaller diameter SiNWs⁷, have also shown a direct-to-indirect bandgap transition, which can potentially be used for laser applications. At the same time, it has also been found that surface passivation of the GaAsNW with $\text{Al}_x\text{Ga}_{1-x}\text{As}$ increases the photoluminescence (PL) lifetime, and minority carrier diffusion lengths, significantly^{8,9}. The bandgap in GeNWs is also found to be dependent upon the type of surface passivation as well as strain¹⁰, which has a consequence on the optoelectronic response of the NW. Concomitantly, GaAs p-i-n NW structures have also shown excellent solar power harvesting capability¹¹. The above results (as well as several references contained therein) highlight the significance of obtaining a detailed understanding of the photo response of NWs and 1D devices. As these nanostructures are being used for image photo detectors, calculations of the photo current response become important. Of particular importance is the behavior of smaller diameter NWs, in keeping with the trend towards smaller feature sizes. Over the years several theoretical work have been reported to understand the optoelectronic response of NWs^{12,13}. Just to name a few advanced works in the field of NEGF coupled to photonic field which recently appeared are the works of Aerberhard et al.^{14,15}, Steiger¹⁶ and Henrickson et al.¹⁷ and Stewart et.al¹⁸ which use either Tight Binding(TB) or bulk 2D $\mathbf{k} \cdot \mathbf{p}$ modeling. The limitation of the TB is the system size, whereas the limitation of the bulk 2D $\mathbf{k} \cdot \mathbf{p}$ system is applicability to 2D systems such as quantum wells, superlattices. In this work we discuss an approach suitable for modeling the photo current response of sub-10 nm diameter NWs. The basis of our work is the band structure calculation by utilizing a 1D 4x4 $\mathbf{k} \cdot \mathbf{p}$ model, with transport calculations utilizing non-equilibrium Green's function (NEGF) formalism. For small structures, semiclassical simulations, such as Monte Carlo, are reasonably accurate, but they may not capture the details of charge distribution in its entirety, particularly in the problem being addressed. On the other hand, NEGF based quantum mechanical approach may provide a more accurate

estimation especially in the phase-coherent regime. Moreover, NEGF allows to incorporate phase-breaking(not considered here) processes via self-energies. To our knowledge this is the first work which couples 4x4 $\mathbf{k} \cdot \mathbf{p}$ and NEGF to compute the photo response of the 1D nanostructures. We have used 4x4 $\mathbf{k} \cdot \mathbf{p}$ (applicable to direct band gap materials) to keep things simple, although conceptually there is no restriction and the model can be easily transferred to the indirect band-gap materials such as Si, Ge by using a larger dimensional $\mathbf{k} \cdot \mathbf{p}$ such as 15x15, 24x24, 30x30 $\mathbf{k} \cdot \mathbf{p}$ models for sub-10 nm 1D devices. This approach takes into account correlations between different band indices as well as spatial correlation allowing us to study the effect of non-locality of electron-photon self-energy. We believe that the proposed method provides a good compromise between computational speed and modeling complexity. The paper is divided into different sections. Section II focuses on the theory, particularly band structure calculation, electron-photon interaction, transport formalism, as well as mode-space approach and physical observables. Device setup and numerical parameters are discussed in Section III. Section IV comprises of results and discussion, and conclusions are drawn in Section V.

II. THEORY

A. Hamiltonian

Starting point of the work was the calculation of the band structure using the original Kane¹⁹ 4x4 $\mathbf{k} \cdot \mathbf{p}$ scheme and using GaAs as a representative material. For the computation of the photoresponse (discussed below), we use a modified 2x2 scheme (or two subband model). Originally $\mathbf{k} \cdot \mathbf{p}$ was done for the direct bandgap materials, although usage of it has been extended to indirect bandgap materials (Si and Ge)^{20–25}, and one can adapt the present method to originally indirect bulk materials.

Hamiltonian is given in basis of cell-periodic zone centered ($\mathbf{k}=0$) Bloch functions $|u_j\rangle = \{|S \uparrow\downarrow\rangle, |X \uparrow\downarrow\rangle, |Y \uparrow\downarrow\rangle, |Z \uparrow\downarrow\rangle\}$ ²⁶

$$\mathbf{H}_{0,bulk} = \begin{pmatrix} E_g + \gamma_a(k_x^2 + k_y^2 + k_z^2) & iPk_x & iPk_y & iPk_z \\ -iPk_x & Lk_x^2 + M(k_y^2 + k_z^2) & Nk_xk_y & Nk_xk_z \\ -iPk_y & Nk_xk_y & Lk_y^2 + M(k_x^2 + k_z^2) & Nk_yk_z \\ -iPk_z & Nk_xk_z & Nk_yk_z & Lk_z^2 + M(k_x^2 + k_y^2) \end{pmatrix} \quad (\text{II.1})$$

where $\gamma_a = \frac{\hbar^2}{2m_0} + F$, F is the effect of remote bands¹⁹, $E_p = 2m_0P^2/\hbar^2$ and

$$L = -\frac{\hbar^2}{2m_0}(\gamma_1 + 4\gamma_2) \quad (\text{II.2})$$

$$M = -\frac{\hbar^2}{2m_0}(\gamma_1 - 2\gamma_2) \quad (\text{II.3})$$

$$N = -\frac{\hbar^2}{2m_0}6\gamma_3 \quad (\text{II.4})$$

with $\gamma_1, \gamma_2, \gamma_3$ being modified Luttinger parameters are related to the original Luttinger parameters $(\gamma_1^L, \gamma_2^L, \gamma_3^L)$ by

$$\gamma_1 = \gamma_1^L - \frac{E_p}{3E_G} \quad (\text{II.5})$$

$$\gamma_2 = \gamma_2^L - \frac{E_p}{6E_G} \quad (\text{II.6})$$

$$\gamma_3 = \gamma_3^L - \frac{E_p}{6E_G} \quad (\text{II.7})$$

where $(E_p, E_G, \gamma_1^L, \gamma_2^L, \gamma_3^L)^{27}$ are specific material parameters. Renormalisation is required so

as to subtract effects of conduction band in the original 3x3 $\mathbf{k} \cdot \mathbf{p}$ model²⁸. Making transformation from k -space representation to real space representation one has to use momentum operators which are given by

$$k_x = -i\hbar \frac{\partial}{\partial x}, k_y = -i\hbar \frac{\partial}{\partial y}, k_z = -i\hbar \frac{\partial}{\partial z} \quad (\text{II.8})$$

Since sine waves naturally satisfy infinite barrier boundary conditions, they are chosen as basis functions in the transverse direction. This corresponds to the situation of free-standing p-i-n junction. Along the transport direction (x -axis) we adopt the following basis functions

$$\chi_i(x) = \frac{1}{\sqrt{\Delta}}(\Theta(x - x_i) - \Theta(x - x_{i+1})) \quad (\text{II.9})$$

where Θ is the Heaviside function, and Δ is the interlayer spacing. Electronic wavefunction in the aforementioned basis is written as

$$|\Psi\rangle = \sum_{j,p,q,i} a_{j,p,q}(x) \sin(k_p y) \sin(k_q z) \chi_i(x) |u_j\rangle = \sum_{j,p,q,i} a_{j,p,q}(x) |j, p, q, i\rangle \quad (\text{II.10})$$

where $j = \{1, 2, 3, 4\}$, $p = 1..N_p$, $q = 1..N_q$ and $k_p = \frac{p\pi}{L_y}$, $k_q = \frac{q\pi}{L_z}$, $i = 1..N_x$ with p denoting y and q denoting z . The total Hamiltonian²⁹ in basis $|j, p, q, i\rangle$

$$\mathbf{H}_{tot} = \begin{pmatrix} \mathbf{H}_1 & \mathbf{W} & 0 & \dots & 0 \\ \mathbf{W}^\dagger & \mathbf{H}_2 & \mathbf{W} & \dots & 0 \\ 0 & \mathbf{W}^\dagger & \mathbf{H}_3 & \ddots & 0 \\ 0 & \dots & \ddots & \ddots & \mathbf{W} \\ 0 & \dots & 0 & \mathbf{W}^\dagger & \mathbf{H}_{N_x} \end{pmatrix} \quad (\text{II.11})$$

where \mathbf{H}_i is the block matrix of the size $4N_p N_q$ and given by

$$\mathbf{H}_i = \begin{pmatrix} \mathbf{H}_{\{1,1\},\{1,1\}} & \mathbf{H}_{\{1,1\},\{1,2\}} & \dots & \dots & \mathbf{H}_{\{1,1\},\{N_p,N_q\}} \\ \mathbf{H}_{\{1,2\},\{1,1\}} & \dots & \dots & \dots & \mathbf{H}_{\{1,2\},\{N_p,N_q\}} \\ \dots & \dots & \mathbf{H}_{\{p,q\},\{p',q'\}} & \dots & \dots \\ \dots & \dots & \dots & \dots & \dots \\ \mathbf{H}_{\{N_p,N_q\},\{1,1\}} & \dots & \dots & \mathbf{H}_{\{N_p,N_q\},\{N_p,N_q-1\}} & \mathbf{H}_{\{N_p,N_q\},\{N_p,N_q\}} \end{pmatrix} \quad (\text{II.12})$$

with

$$\mathbf{H}_{(p,q),(p',q')} = \mathbf{H}_{(p,q),(p',q')}^{0,d} + \mathbf{H}_{(p,q),(p',q')}^{0,c} + \mathbf{H}_{(p,q),(p',q')}^{0,cv} + \mathbf{V}(i)_{(p,q),(p',q')} \quad (\text{II.13})$$

$$\mathbf{H}_{(p,q),(p',q')}^{0,d} = \delta_{p,p'} \delta_{q,q'} \begin{pmatrix} \gamma_a(\frac{2}{\Delta^2} + k_p^2 + k_q^2) + E_g & 0 & 0 & 0 \\ 0 & L\frac{2}{\Delta^2} + M(k_p^2 + k_q^2) & 0 & 0 \\ 0 & 0 & Lk_p^2 + M(\frac{2}{\Delta^2} + k_q^2) & 0 \\ 0 & 0 & 0 & Lk_q^2 + M(\frac{2}{\Delta^2} + k_p^2) \end{pmatrix} \quad (\text{II.14})$$

$$\mathbf{H}_{(p,q),(p',q')}^{0,c} = \begin{pmatrix} 0 & 0 & P\delta_{q,q'} \frac{4k_{p'}p}{\pi(p^2 - p'^2)} \delta_{p+p',odd} & P\delta_{p,p'} \frac{4k_{q'}q}{\pi(q^2 - q'^2)} \delta_{q+q',odd} \\ 0 & 0 & 0 & 0 \\ -P\delta_{q,q'} \frac{4k_{p'}p}{\pi(p^2 - p'^2)} \delta_{p+p',odd} & 0 & 0 & 0 \\ -P\delta_{p,p'} \frac{4k_{q'}q}{\pi(q^2 - q'^2)} \delta_{q+q',odd} & 0 & 0 & 0 \end{pmatrix} \quad (\text{II.15})$$

$$\mathbf{H}_{(p,q),(p',q')}^{0,cv} = -N \left(\frac{4k_{p'}p}{\pi(p^2 - p'^2)} \right) \left(\frac{4k_{q'}q}{\pi(q^2 - q'^2)} \right) \delta_{p+p',odd} \delta_{q+q',odd} \begin{pmatrix} 0 & 0 & 0 & 0 \\ 0 & 0 & 0 & 0 \\ 0 & 0 & 0 & 1 \\ 0 & 0 & 1 & 0 \end{pmatrix} \quad (\text{II.16})$$

where δ is the Kronecker delta and $\delta_{p+p',odd} = \{1, \text{ if } p + p' = \text{odd}, \text{ otherwise } 0\}$ and

$$\mathbf{V}(i)_{\{p,q\},\{p',q'\}} = \mathbf{I}_{4 \times 4} \frac{4}{L_y L_z} \int_0^{L_y} \int_0^{L_z} \sin(k_{p'} y) \sin(k_{q'} z) \phi(x = x_i; y, z) \sin(k_p y) \sin(k_q z) dy dz \quad (\text{II.17})$$

is orthogonal transformation to $|j, p, q, i\rangle$ of Hartree $\phi(x = x_i; y, z)$ potential (which is obtained self-consistently solving NEGF-Poisson equation), with $\mathbf{I}_{4 \times 4}$ being the 4x4 identity matrix. Similarly, the inter-layer coupling matrix can be written in similar manner

$$\mathbf{W}_{(p,q),(p',q')} = \mathbf{W}_{(p,q),(p',q')}^d + \mathbf{W}_{(p,q),(p',q')}^c \quad (\text{II.18})$$

, where

$$\mathbf{W}_{(p,q),(p',q')}^d = \delta_{p,p'} \delta_{q,q'} \begin{pmatrix} \frac{-\gamma_a}{\Delta^2} & \frac{P}{2\Delta} & 0 & 0 \\ \frac{-P}{2\Delta} & \frac{-L}{\Delta^2} & 0 & 0 \\ 0 & 0 & \frac{-M}{\Delta^2} & 0 \\ 0 & 0 & 0 & \frac{-M}{\Delta^2} \end{pmatrix} \quad (\text{II.19})$$

$$\mathbf{W}_{(p,q),(p',q')}^c = \begin{pmatrix} 0 & 0 & 0 & 0 \\ 0 & 0 & \frac{-N}{2\Delta} \frac{4k_{p'}p}{\pi(p^2 - p'^2)} \delta_{p+p',odd} \delta_{q,q'} & \frac{-N}{2\Delta} \frac{4k_{q'}q}{\pi(q^2 - q'^2)} \delta_{q+q',odd} \delta_{p,p'} \\ 0 & \frac{-N}{2\Delta} \frac{4k_{p'}p}{\pi(p^2 - p'^2)} \delta_{p+p',odd} \delta_{q,q'} & 0 & 0 \\ 0 & \frac{-N}{2\Delta} \frac{4k_{q'}q}{\pi(q^2 - q'^2)} \delta_{q+q',odd} \delta_{p,p'} & 0 & 0 \end{pmatrix} \quad (\text{II.20})$$

One should mention that k_p, k_q form rectangular grid. Further simplification such as Hamiltonian size reduction in $\mathbf{k} \cdot \mathbf{p}$ basis by taking only k_p, k_q vectors inside the circle²⁹ can be done to minimize memory usage and computational power. Moreover, one can get further matrix size reduction by employing the mode-space approach. Mode-space is crucial for the recursive algorithm in NEGF implementation and charge distribution construction. It was shown³⁰ that in case of electron-photon interaction one cannot easily use recursive approach since self-energies are highly non-local and in this case one has to take more off-diagonal

blocks. In other words, more correlations between electron Green's functions have to be kept when dealing with electron photon interaction.

B. Electron-photon interaction. Monochromatic excitation.

The electron-photon interaction part of Hamiltonian reads as

$$H_{e-ph} = -\frac{e}{m_0} \mathbf{A} \cdot \mathbf{p} \quad (\text{II.21})$$

where the photon field is quantized and is given by

$$\mathbf{A} = \sum_{\lambda, \mathbf{q}} \left[\mathbf{A}_0(\lambda, \mathbf{q}) \mathbf{b}_{\lambda, \mathbf{q}} e^{i\omega_\lambda t} + \mathbf{A}_0(\lambda, -\mathbf{q}) \mathbf{b}_{\lambda, -\mathbf{q}}^\dagger e^{-i\omega_\lambda t} \right] e^{i\mathbf{q}\mathbf{r}} \quad (\text{II.22})$$

$$\mathbf{A}_0(\lambda, \mathbf{q}) = \mathbf{e}_{\lambda, \mathbf{q}} \sqrt{\frac{\hbar^2}{2\epsilon_0 E_\lambda V}} \quad (\text{II.23})$$

where $\mathbf{b}_{\lambda, \mathbf{q}}^\dagger, \mathbf{b}_{\lambda, \mathbf{q}}$ are the photon creation and annihilation operators, respectively, $\mathbf{e}_{\lambda, \mathbf{q}}$ is the polarization vector, \mathbf{q} is the photon wavevector and λ is the photon energy. Sum is over all photon wavevectors and energies. where V is the absorbing volume. The incident photon flux is related to photon occupation number via

$$\Phi_\lambda = \frac{N_\lambda c}{V \sqrt{\mu\epsilon}} = \frac{I_\lambda}{E_\lambda} \quad (\text{II.24})$$

where I_λ is the intensity of the EM field and c is the speed of light. Equation (II.21) in the second quantized form can be written as

$$H_{e-ph} = - \sum_{(j, p, q, i), (j', p', q', i')} \langle j', p', q', i' | \mathbf{A} \cdot \mathbf{p} | j, p, q, i \rangle c_{j', p', q', i'}^\dagger c_{j, p, q, i} (b e^{i\omega_\lambda t} + b^\dagger e^{-i\omega_\lambda t}) \quad (\text{II.25})$$

with $c_{j', p', q', i'}^\dagger$ - being electron creation operator in the state symmetry j' , transverse subband $\{p', q'\}$, and position $x_{i'}$ and $c_{j, p, q, i}$ - being electron destruction operator in the state of symmetry j , transverse subband $\{p, q\}$, and position x_i .

Carrying out explicitly matrix element of (II.25) in dipole approximation with wire dimensions much smaller than a wavelength ($\mathbf{q}\mathbf{r} \ll 1$) and taking into account only inter-subband excitations (CB-VB), i.e. considering only CB-VB transitions, we arrive at

$$M_{\{j, p, q, i\}, \{j', p', q', i'\}} = \langle j', p', q', i' | \mathbf{A} \cdot \mathbf{p} | j, p, q, i \rangle = \delta_{p, p'} \delta_{q, q'} \delta_{i, i'} \mathbf{A} \cdot \mathbf{p}_{i, \{j, j'\}} \quad (\text{II.26})$$

where

$$\mathbf{p}_{i,\{j,j'\}} = \{\langle S \uparrow \downarrow | p_x | X \uparrow \downarrow \rangle, \langle S \uparrow \downarrow | p_y | Y \uparrow \downarrow \rangle, \langle S \uparrow \downarrow | p_z | Z \uparrow \downarrow \rangle\} \quad (\text{II.27a})$$

$$\langle S \uparrow \downarrow | p_x | X \uparrow \downarrow \rangle = \langle S \uparrow \downarrow | p_y | Y \uparrow \downarrow \rangle = \langle S \uparrow \downarrow | p_z | Z \uparrow \downarrow \rangle = \frac{m_0}{\hbar} iP \quad (\text{II.27b})$$

Total Matrix (\mathbf{M}_{e-ph}) becomes

$$\mathbf{M}_{e-ph}^{\{x,y,z\}} = A_0 \frac{m_0}{\hbar} \begin{pmatrix} \mathbf{M}_{(1,1)(1,1)}^{\{x,y,z\}} & 0 & \dots & \dots & 0 \\ 0 & 0 & \dots & \dots & 0 \\ \dots & \dots & 0 & \dots & \dots \\ \dots & 0 & \mathbf{M}_{(p,q)(p,q)}^{\{x,y,z\}} & \dots & \dots \\ \dots & 0 & 0 & \dots & 0 \\ 0 & \dots & \dots & 0 & \mathbf{M}_{(N_p N_q)(N_p N_q)}^{\{x,y,z\}} \end{pmatrix} \quad (\text{II.28})$$

where,

$$\mathbf{M}_{(p,q)(p,q)}^x = \begin{pmatrix} 0 & iP & 0 & 0 \\ -iP & 0 & 0 & 0 \\ 0 & 0 & 0 & 0 \\ 0 & 0 & 0 & 0 \end{pmatrix} \quad (\text{II.29})$$

$$\mathbf{M}_{(p,q)(p,q)}^y = \begin{pmatrix} 0 & 0 & iP & 0 \\ 0 & 0 & 0 & 0 \\ -iP & 0 & 0 & 0 \\ 0 & 0 & 0 & 0 \end{pmatrix} \quad (\text{II.30})$$

$$\mathbf{M}_{(p,q)(p,q)}^z = \begin{pmatrix} 0 & 0 & 0 & iP \\ 0 & 0 & 0 & 0 \\ 0 & 0 & 0 & 0 \\ -iP & 0 & 0 & 0 \end{pmatrix} \quad (\text{II.31})$$

$$\mathbf{M}_{(p,q)(p,q)}^{\{l.c.\}} = \begin{pmatrix} 0 & iP & iP & iP \\ -iP & 0 & 0 & 0 \\ -iP & 0 & 0 & 0 \\ -iP & 0 & 0 & 0 \end{pmatrix} \quad (\text{II.32})$$

where x,y,z stands for either x,y or z EM field polarization, l.c. stands for the linear polarization which is linear combination of the x,y and z axis.

C. NEGF and Self-Energies

Green's functions are assumed to be in steady state with electron Green's function being at zero temperature (although temperature comes via Fermi levels) and photon Green's functions being unperturbed by electronic elementary excitations. Within Keldysh formalism the Dyson's equations of motion for the electronic Green's functions in matrix notation are given by

$$\mathbf{G}^R(E) = ((E + i\gamma)\mathbf{I} - \mathbf{H}_{tot}(E) - \mathbf{\Sigma}^B(E) - \mathbf{\Sigma}_{e-ph}(E))^{-1} \quad (\text{II.33a})$$

$$\mathbf{G}^<(E) = \mathbf{G}^R(E) \{ \mathbf{\Sigma}^{<,B}(E) + \mathbf{\Sigma}_{e-ph}^{<}(E) \} \mathbf{G}^A(E) \quad (\text{II.33b})$$

$$\mathbf{G}^A(E) = [\mathbf{G}^R(E)]^\dagger \quad (\text{II.33c})$$

$$\mathbf{G}^>(E) = \mathbf{G}^R(E) - \mathbf{G}^A(E) + \mathbf{G}^<(E) \quad (\text{II.33d})$$

where $\mathbf{\Sigma}^B(E)$ is the boundary self-energy, which incorporates effect of semi-infinite contact(coupling to contacts). Contacts are assumed to be with equilibrium with right and left leads respectively and are perfect absorbers³¹. $\mathbf{\Sigma}_{e-ph}(E)$ is the electron-photon self-energy describing electron-photon interaction, where

$$\mathbf{\Sigma}^B(E) \equiv \mathbf{\Sigma}^B(E) = \begin{pmatrix} \mathbf{\Sigma}_L^B(E) & 0 & \dots & 0 \\ 0 & 0 & \dots & 0 \\ \dots & \dots & \dots & 0 \\ 0 & \dots & 0 & \mathbf{\Sigma}_R^B(E) \end{pmatrix} \quad (\text{II.34})$$

where $\mathbf{\Sigma}_{L,R}^B(E)$ are the block matrices of size $4N_p N_q$ that are related to surface Green's functions via

$$\mathbf{\Sigma}_L^B(E) = \mathbf{W} \mathbf{g}_L(E) \mathbf{W}^\dagger \quad (\text{II.35a})$$

$$\mathbf{\Sigma}_R^B(E) = \mathbf{W}^\dagger \mathbf{g}_R(E) \mathbf{W} \quad (\text{II.35b})$$

where,

$$\mathbf{g}_L(E) = [E - \mathbf{H}_1 - \mathbf{W}^\dagger \mathbf{g}_L(E) \mathbf{W}]^{-1} \quad (\text{II.36a})$$

$$\mathbf{g}_R(E) = [E - \mathbf{H}_{N_x} - \mathbf{W} \mathbf{g}_R(E) \mathbf{W}^\dagger]^{-1} \quad (\text{II.36b})$$

are surface Green's functions corresponding to left and right lead, respectively. Equations on the $\mathbf{g}_L(E), \mathbf{g}_R(E)$ are matrix quadratic equations. There are many ways of calculating the

solution to (II.36). Simplest solution is just straightforward iteration, although this is very slowly converging process. Therefore, we have adopted the improved version of Anderson mixing³² which is also simple in implementation. Lesser(in-scattering) boundary self energy in case of equilibrated contacts is given by

$$\Sigma_{L,R}^{<,B}(E) = i\Gamma_{L,R}(E)f_{L,R} \quad (\text{II.37a})$$

$$\Gamma_{L,R}(E) = i(\Sigma_{L,R}^B(E) - \Sigma_{L,R}^{B,\dagger}(E)) \quad (\text{II.37b})$$

where $f_{L,R}$ are the Fermi levels at the left and right lead respectively, and $\Gamma_{L,R}$ is the level broadening.

Light-matter interaction leads to electron-hole pair generation and electron-hole recombination by absorbing/emitting a photon. This process is inelastic, and in general is phase-breaking. In order to incorporate this interaction into NEGF formalism in the first order Born-approximation(one-photon processes) one has to utilize Wick's theorem and Langreth contour rules as it was done in several works^{16,33} and in the original Henrickson's¹⁷ papers.

Most self-energies of this form, including electron-photon,(fermion-boson interaction in the limit one elementary excitation) are current conserving³⁴. In order to achieve current conservation one has to utilize self consistency among Green's functions and self-energies - in other words use self-consistent Born approximation(SCBA) or one can use current conserving schemes using Non-self consistent Born Approximation described in Lake³⁵ et.al. A detailed derivation of the self-consistent Born approximation approach is given in the work of Jiang et al.³⁶. Lesser and greater parts, $\Sigma_{E-ph}^{<,>}$ are given by

$$\Sigma_{e-ph}^{<,>}(x, x', E) = \Sigma_{e-ph}^{<,>,abs}(E) + \Sigma_{e-ph}^{<,>,em}(E) + \Sigma_{e-ph}^{<,>,sp}(E) \quad (\text{II.38a})$$

$$\Sigma_{e-ph}^{<,>,abs}(E) = N_\lambda \mathbf{M}_{e-ph} \mathbf{G}^{<,>}(E \mp \hbar\omega) \mathbf{M}_{e-ph} \quad (\text{II.38b})$$

$$\Sigma_{e-ph}^{<,>,em}(E) = N_\lambda \mathbf{M}_{e-ph} \mathbf{G}^{<,>}(E \pm \hbar\omega) \mathbf{M}_{e-ph} \quad (\text{II.38c})$$

$$\Sigma_{e-ph}^{<,>,sp}(E) = \mathbf{M}_{e-ph} \left(\int_{E_{\min}}^{E_{\max}} d(\hbar\omega_\gamma) \mathbf{G}^{<,>}(E \pm \hbar\omega_\gamma) \right) \mathbf{M}_{e-ph} \quad (\text{II.38d})$$

where $\Sigma_{e-ph}^{<,>,abs}$, $\Sigma_{e-ph}^{<,>,em}$, $\Sigma_{e-ph}^{<,>,sp}$ are the self energies associated with photon absorption, stimulated emission and spontaneous emission, respectively. The derivation is very similar to the work of Jiang et al.³⁷ One should note that spontaneous emission term is integrated over broad energy range in CB and VB energy regions and is only dependent on joint density

of states and occupation numbers at energies which differs by photon energy. E_{min}, E_{max} are the minimal and maximal photon energies dictated by material and device parameters. \mathbf{M}_{e-ph} is the full electron-photon interaction Hamiltonian in the basis $|j, p, q, i\rangle$. Strictly speaking, one has to be careful considering \mathbf{M}_{e-ph} since originally it couples only bulk CB-VB bands. In other words, if one wants to consider inter-subband excitations such as CB-CB or VB-VB (either within CB or VB manifolds), the \mathbf{M}_{e-ph} has to be modified accordingly to include intraband coupling in the original bulk model since one 3D band gives rise to many 1D subbands. In case of short-channel devices under certain biases the spontaneous term is assumed to be small¹⁴ and as will be shown later can be neglected. Real part of the retarded Σ_{e-ph} self energy is neglected since it leads just to energy renormalization¹⁴, and only imaginary part of the Σ_{e-ph} is important and given by ((x, x') notation is omitted throughout for simplicity)

$$Im(\Sigma_{e-ph}(E)) = \frac{1}{2}(\Sigma_{e-ph}^>(E) - \Sigma_{e-ph}^<(E)) \quad (\text{II.39})$$

D. Mode space and Physical quantities

In case of mode-space²⁹ transformation one defines mode m in the following manner

$$\Phi_m(x_i, y_j, z_k) = \sum_{j,p,q} \alpha_{j,p,q}^m(i) |p, q, j\rangle \quad (\text{II.40})$$

which satisfies 2D-sliced Schrodinger equation at slice i

$$(\mathbf{H}_i + \mathbf{W} + \mathbf{W}^\dagger)\Phi_m(x_i, y_j, z_k) = E_m \Phi_m(x_i, y_j, z_k) \quad (\text{II.41})$$

Original eigenfunction of (II.10) is given in terms of modes as

$$|\Psi\rangle = \sum_m Y_m(x_i) \Phi_m(x_i, y_j, z_k) \quad (\text{II.42})$$

In order to have self-consistent NEGF with Poisson one has to compute 3D electron density in the real space representation. An incomplete³⁸ calculation consists of writing 3D electron density in real space³⁹ neglecting the mode correlation effects as

$$\begin{aligned} n_{3D}^{rs}(i, j, k) &= \frac{-2i}{\Delta\Delta_y\Delta_z} \int \frac{dE}{2\pi} (\mathbf{U}_K \mathbf{U}_M \mathbf{G}^{<,ms}(x, x', E) \mathbf{U}_M^\dagger \mathbf{U}_K^\dagger)_{\{i,j,k\},\{i,j,k\}} \simeq \\ &\simeq \alpha \sum_{n=1}^{N_m} \int \frac{dE}{2\pi} G_{(i,n),(i,n)}^{<,ms}(E) \left| \sum_{j,p,q} \sin(k_p y_j) \sin(k_q z_k) \alpha_{j,p,q}^n(i) \right|^2 \end{aligned} \quad (\text{II.43})$$

where $\alpha = \frac{-2i}{\Delta\Delta_y\Delta_z} \frac{4}{N_yN_z}$, rs, ms superscripts stand for the real-space and mode-space representations respectively. $G_{(i,n),(i,n)}^{<,ms}$ stands for the diagonal matrix element of mode n at block i . $\mathbf{U}_K, \mathbf{U}_M$ are unitary transformation matrices²⁹ defined as block diagonal matrices built from $\mathbf{U}_k, \mathbf{U}_m(i)$ respectively, where

$$\mathbf{U}_k = \frac{2}{\sqrt{N_yN_z}} \begin{pmatrix} \sin(k_1y_1)\sin(k_1z_1)\mathbf{I}_{4x4} & \dots & \sin(k_1z_1)\sin(k_{N_q}z_1)\mathbf{I}_{4x4} & \dots & \sin(k_{N_p}y_1)\sin(k_{N_q}z_1)\mathbf{I}_{4x4} \\ \sin(k_1y_1)\sin(k_1z_2)\mathbf{I}_{4x4} & \dots & \sin(k_1y_1)\sin(k_{N_q}z_2)\mathbf{I}_{4x4} & \dots & \sin(k_{N_p}y_1)\sin(k_{N_q}z_2)\mathbf{I}_{4x4} \\ \dots & \ddots & \dots & \dots & \dots \\ \sin(k_1y_1)\sin(k_1z_N)\mathbf{I}_{4x4} & \dots & \sin(k_1y_1)\sin(k_{N_q}z_N)\mathbf{I}_{4x4} & \dots & \sin(k_{N_p}y_1)\sin(k_{N_q}z_N)\mathbf{I}_{4x4} \\ \dots & \dots & \dots & \ddots & \dots \\ \sin(k_1y_M)\sin(k_1z_N)\mathbf{I}_{4x4} & \dots & \dots & \dots & \sin(k_{N_p}y_M)\sin(k_{N_q}z_N)\mathbf{I}_{4x4} \end{pmatrix} \quad (\text{II.44})$$

is the size of $(4NM) \times (4N_pN_q)$ and

$$\mathbf{U}_m(i) = \begin{pmatrix} \alpha_{1,1,1}^1(i) & \alpha_{1,1,1}^2(i) & \dots & \dots & \alpha_{1,1,1}^{N_m}(i) \\ \alpha_{2,1,1}^1(i) & \alpha_{2,1,1}^2(i) & \dots & \dots & \dots \\ \dots & \dots & \dots & \dots & \dots \\ \dots & \dots & \alpha_{j,N_p,N_q}^n(i) & \dots & \dots \\ \alpha_{4,N_p,N_q}^1(i) & \alpha_{4,N_p,N_q}^2(i) & \dots & \dots & \alpha_{4,N_p,N_q}^{N_m}(i) \end{pmatrix} \quad (\text{II.45})$$

is the size of $(4N_pN_q) \times N_m$

Current flowing between layers i , and $i+1$ can be written as

$$I_{x_i \rightarrow x_{i+1}} = \frac{2e}{\hbar} \int \frac{dE}{2\pi} \text{tr} \{ \mathbf{W}^{ms} \mathbf{G}_{i,i+1}^{<,ms} - \mathbf{W}^{\dagger,ms} \mathbf{G}_{i+1,i}^{<,ms} \} \quad (\text{II.46})$$

Similar approach has been applied in the study of thermal expansion of single-wall carbon nanotubes and grapheme sheets⁴⁰

III. NUMERICAL DETAILS

The device under study is a p-i-n structure and is depicted in Fig. 1. The device is 42 nm long, with a square cross-section of 10nm x 10nm. The doping on both the n and p ends is assumed to be $3.2 * 10^{18} \text{ cm}^{-3}$. Furthermore, length of the p and n region was set $L_p = L_n = 12\text{nm}$ and inter-layer spacing $\Delta = 0.3\text{nm}$. Current conserving grid was chosen¹⁶

as $\Delta E = E_\lambda/N_{ph}$ with total number of energy grid points $N_{tot} = \text{Int}((|E_1| + |E_2|)/\Delta E)$ with E_1, E_2 being conduction and valence band cut-off energies chosen accordingly to the region of interest. N_{ph} defines by how many energy points separated E and $E + \hbar\omega$. N_{tot} varied between 800 and 2000 points to make sure convergence is achieved in energy space. N_x was set to 140 points. The potential profile is assumed to be uniform in the cross-sectional area. 1D potential profiles and Fermi-levels were obtained by nextnano simulator⁴¹ with the parameters being $E_g=1.42\text{eV}$, $m_c=0.067m_e$, $m_h=0.082m_e$ where parameters are bandgap, effective conduction mass, effective valence mass(light hole) respectively. Although, strictly speaking there is no physical justification for this, but it does not affect the physical picture except consideration of the boundary effects in which we are not interested at the moment. 1D Potential profiles and Quasi-Fermi levels were fed into optical NEGF simulator based on 2 subband model, which is written as

$$\mathbf{H}_{2x2}(E) = \begin{pmatrix} E_g + \frac{\hbar^2}{2m_0} \frac{\gamma_a}{\Delta^2} & 0 \\ 0 & \frac{\hbar^2}{2m_0} \frac{\gamma_l}{\Delta^2} \end{pmatrix} \quad (\text{III.1})$$

$$\mathbf{W}_{2x2}(E) = \begin{pmatrix} -\frac{\hbar^2}{2m_0} \frac{\gamma_a}{\Delta^2} & \frac{P}{2\Delta} \\ -\frac{P}{2\Delta} & -\frac{\hbar^2}{2m_0} \frac{\gamma_l}{\Delta^2} \end{pmatrix} \quad (\text{III.2})$$

In order to avoid spurious solutions in k - space ($\mathbf{k} = (k_x, -i\frac{\partial}{\partial y}, -i\frac{\partial}{\partial z})$) we took cross-sectional area such that condition on the envelope function is satisfied so, that plane-wave expansion lies in the first Brillouin-zone⁴²⁻⁴⁵

$$\frac{2\pi N_{p,q}^{max}}{L_{y,z}} \ll \frac{2\pi}{a} \quad (\text{III.3})$$

with $N_{p,q}^{max} \leq L_{y,z}/a$. In addition we set $\gamma_c = 0$ with optimizing the parameters^{27,46} $\gamma_1, \gamma_2, \gamma_3$ ⁴⁷ such that bulk effective masses of hole and electrons are reproduced. Moreover, the original Hamiltonian can be modified to avoid spurious solutions⁴⁸. Going from k - space representation to real-space representation $(-i\frac{\partial}{\partial x}, -i\frac{\partial}{\partial y}, -i\frac{\partial}{\partial z})$ with finite differences being the basis one has another source of spurious solutions^{49,50}. Such solutions can be avoided by using certain finite element basis⁵⁰. However in general, there is no common remedy for this type of problem⁵⁰. In particular, to avoid this type of problem, one either chooses inter-layer spacing Δ accordingly to the parameters $\gamma_1, \gamma_2, \gamma_3$ ⁴⁹, or as we did, fix the Δ and vary the parameters γ_a, γ_l to reproduce the bulk effective masses of conduction band and light-hole bands (we have assumed that charge carrier effective masses of 10nm x 10nm

are bulk values). Parameters after fitting are $\gamma_a = 8, \gamma_l = -1$. SCBA computations are aborted once convergence is achieved by monitoring the norm of the total photocurrent $\int (I_{ph}^e + I_{ph}^h)_{n+1} dE / \int (I_{ph}^e + I_{ph}^h)_n dE < \epsilon$, where ϵ was set to 10^{-4} . In the computation of the spontaneous emission term, we have set E_{min}, E_{max} to be in the range of $E_\lambda \mp 0.4E_\lambda$, for particular photon energy with $0.4E_\lambda$ term being chosen such that results are converged meanwhile minimizing the computational resources. Laser intensity is assumed to be 100 W/cm^2 unless specified otherwise. The whole structure is uniformly illuminated. EM field polarized along x-axis. Device structure is depicted on the Figure 1.

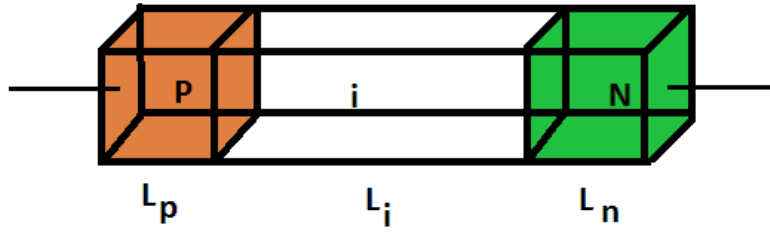


FIG. 1. nanosized p-i-n diode

IV. RESULTS AND DISCUSSION

Figure 2 depicts the conduction and valence band profiles. As can be seen, the built-in potential is $V_{bi} = 1.4 \text{ V}$. In the calculation, we have used non-self-consistent Poisson profile, which deviates from the self-consistent solution by less than 5%⁵¹ at a light intensity $I = 10^5 \text{ W/cm}^2$. Since the light intensity in our work is much smaller, therefore one expects even lower deviation from SCF Poisson profile. Upon light illumination of the diode, the electron-hole pairs start to form, which are then separated by the electric field. Figure 3 shows typical spatial hole and electron current distribution. One can see that total current is conserved, meanwhile hole current grows towards the p -contact and electron current as we move towards the n -contact. To investigate it further we have calculated the current energetic distribution in the device, including left and right leads. Typical spectral current is shown in Fig.4. One clearly sees three regions contributing to the current, with the flat region corresponding to the channel current, and two peaks corresponding to the p -region and n -region currents (flowing just above and below conduction and valence band edges, respectively). The distribution is not symmetric with respect to p and n regions. Figure 5

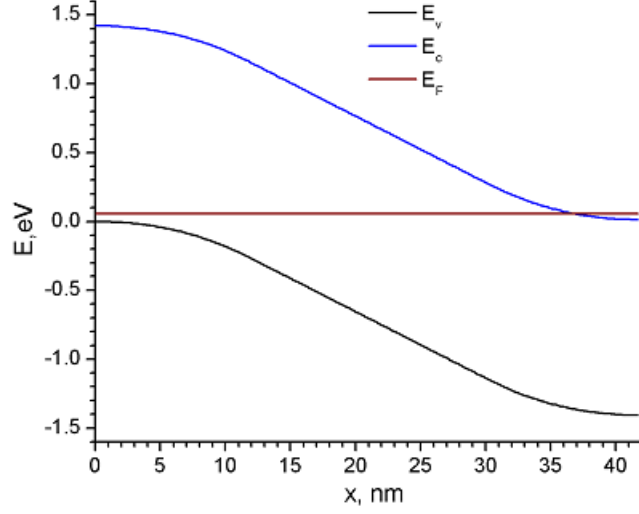


FIG. 2. Band profile for the conduction and valence band. Brown line indicates Fermi level.

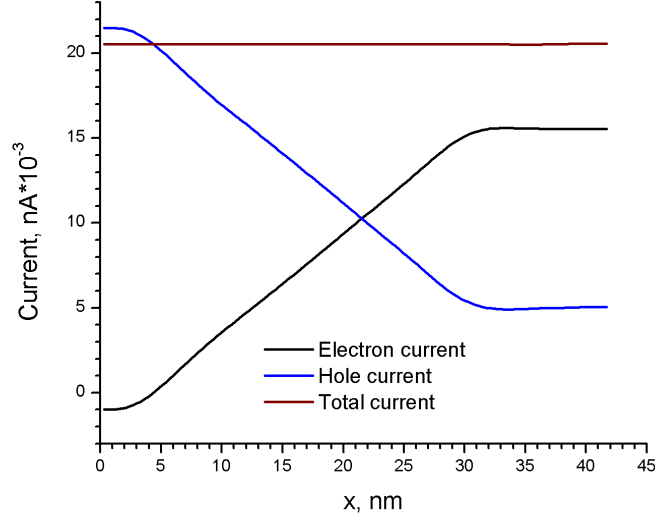


FIG. 3. Spatial distribution of hole and electron current at $E_\lambda = 1.56\text{eV}$ at zero bias for p-i-n structure. One can see that total current is conserved

shows photocurrent in the short circuit(sc) condition at different photon energies. One can see formation of two peaks in the Franz-Keldysh (photon-assisted tunneling or PA) regime and without it. The manifestation of the Franz-Keldysh effect is the non-zero current below fundamental bandgap. In PA regime the first peak is shifted towards lower energies due to

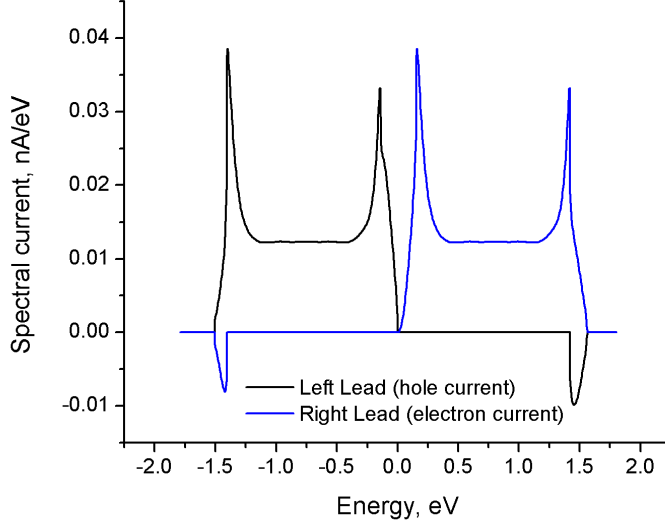


FIG. 4. Energetic current distribution over valence and conduction band at $E_\lambda = 1.56\text{eV}$ at zero bias for p-i-n structure.

non-zero DOS below the bandgap. It is seen that just interband approximation (zero DOS below CB and below VB edges respectively) significantly underestimates the photocurrent. The channel current grows as photon energy increases due to a greater availability of DOS. The local density of states (LDOS) has an oscillatory pattern both in spatial and energetic coordinates as seen in Fig.6 which forms due to incident k_+ and reflected k_- electron waves. By keeping all off-band correlations^{52,53} in the Green's functions, i.e. elements such as $G_{x,x',c,v}^<(E)$ and where spontaneous emission does not play significant role with coherent light⁵⁴ source one has phase-coherent photo-response. This is automatically satisfied in our case, since we are working with the full rank of the matrix.

In addition, it can be seen that spontaneous emission does not play a role in the device of this length, since typical lifetime of the carrier before spontaneously emitting a photon is of the order of nanoseconds which would require much longer device length to experience it. One should mention that under certain bias conditions, it is possible to have spontaneous emission even for the small-sized devices¹⁶. For our system to experience it, one would go beyond 1.4eV as we have checked in the range of our biases, and no contributions have been seen.

The peaks in the photocurrent can be explained through interference, which leads to

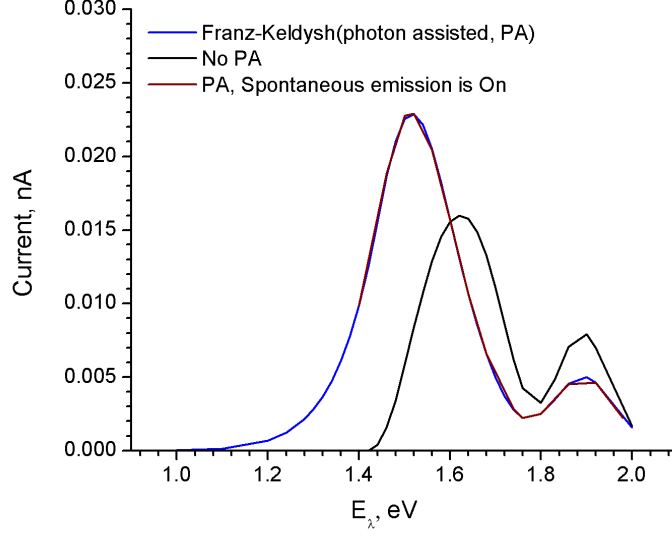


FIG. 5. Photoresponse at zero bias for p-i-n structure with and without photon-assisted (Franz-Keldysh effect) tunneling.

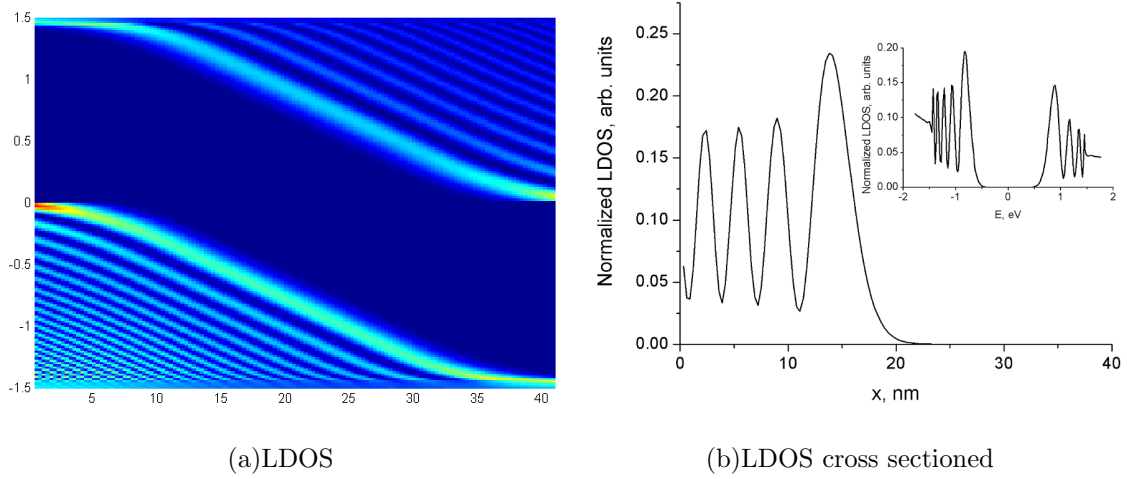


FIG. 6. Local Density of States. a) LDOS plot (x-axis is position in nm, y-axis is energy in eV) b) Cross sections of the LDOS. Main graph is the spatial LDOS near the top of the Valence band. Inset is the cross section over energy coordinate near the middle of the device.

oscillations in the Joint Density of states(JDOS) along energy coordinate.

Figure 7 shows the IV-curve of the diode. Dark current in our case is negligible at given biases and the only current computed is the photo-current. Exponential decay can

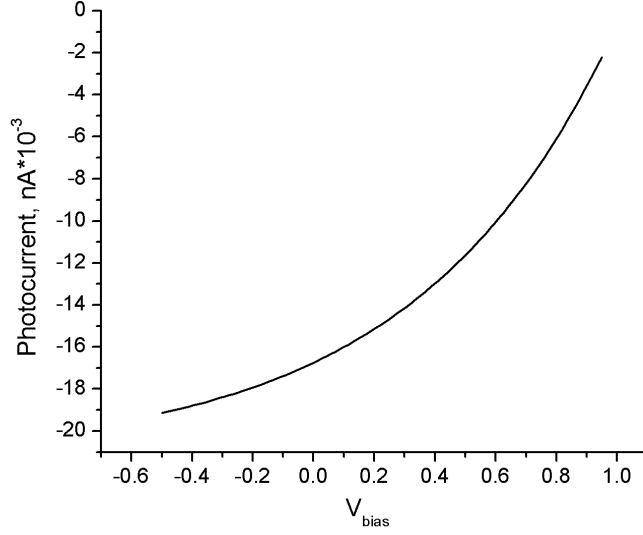


FIG. 7. IV characteristics at $E_\lambda = 1.56\text{eV}$. Please note that the current sign is take opposite of the original one (originally current flow taken positive from p lead to n lead).

be explained in terms of absorption decrease as bias increases. The order of magnitude and IV curve have a reasonable agreement (taking into account just two conducting modes and device dimensions) with the experimental data on the GaAs pn-diode photo-response⁵⁵.

Figure 8 shows 2D spectral currents at different photon energies. One can see that going from $E_\lambda=1.4$ eV to $E_\lambda=1.64$ eV, the channel current increases with respect to band-edge currents due to increase of available DOS. On the other hand, at $E_\lambda=1.76$ eV current in diode flows near band-edges. This phenomenon can be explained by spatial oscillations of LDOS. The photo-current is mainly due to carrier photo-generation and inter-subband recombination. This is more pronounced at Figures 8(e) and 8(f). One can see spatial current oscillations in the valence band, which can also be seen in the energy coordinate. In addition to this, one can see some negative components at contacts. PN Diodes are known for it's rectification properties, which is not the case here and does deteriorate the device performance. The way to bypass this either use potential barriers such as it is done in the work of Henrickson et.al¹⁷ or by using carrier-selective contacts⁵⁶.

These features are also seen on the Figure 9. This is mostly pronounced in Fig. 9(b) and Fig.9(c). In Fig. 9(b) one can see oscillations in the hole and electron current density along the length of the device. Figure 9(c) is richer in features such as curvature change over

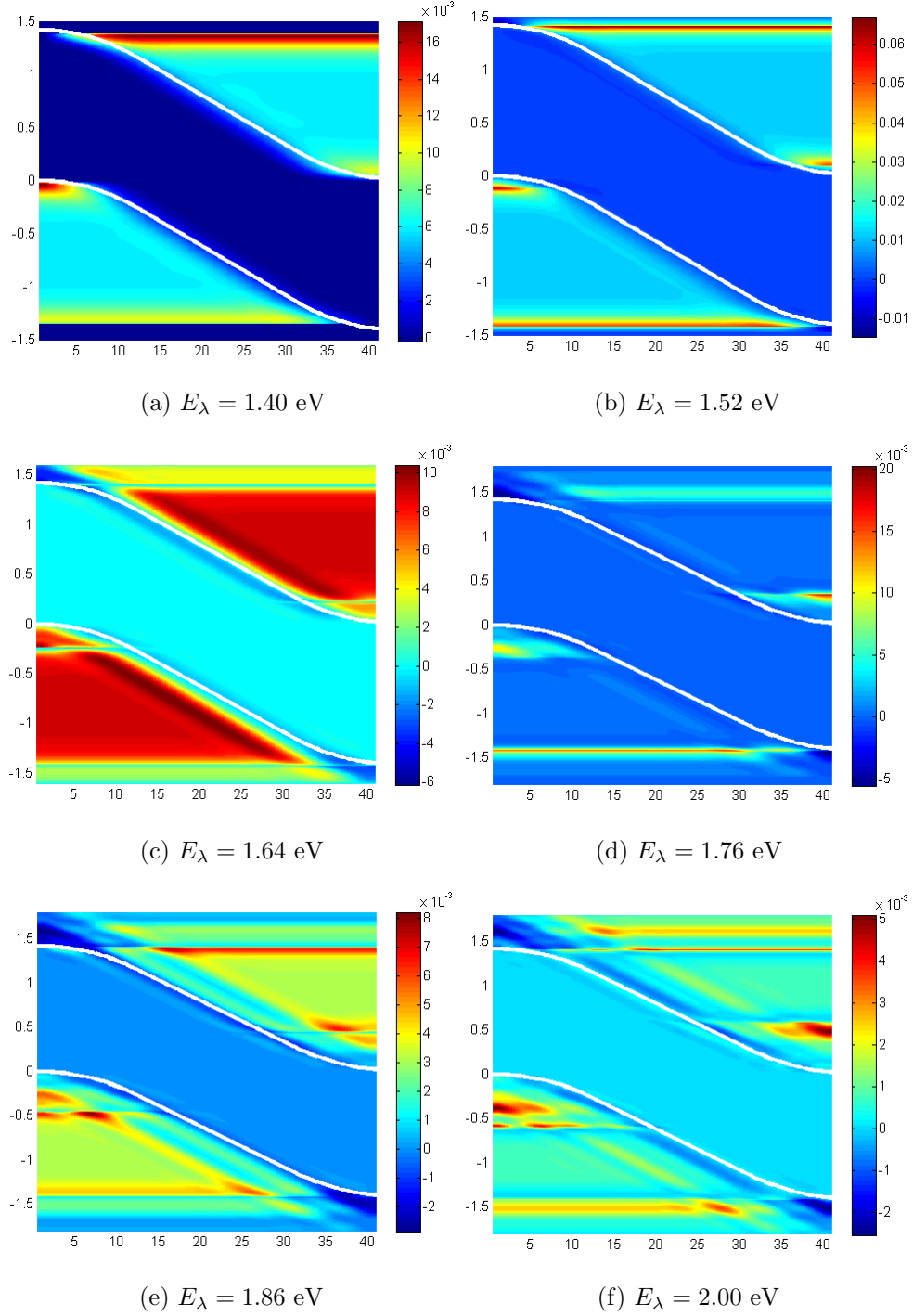
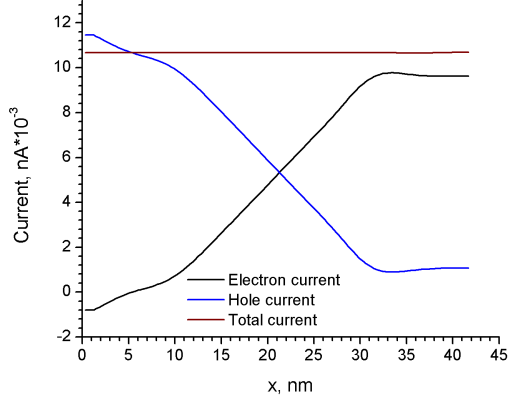
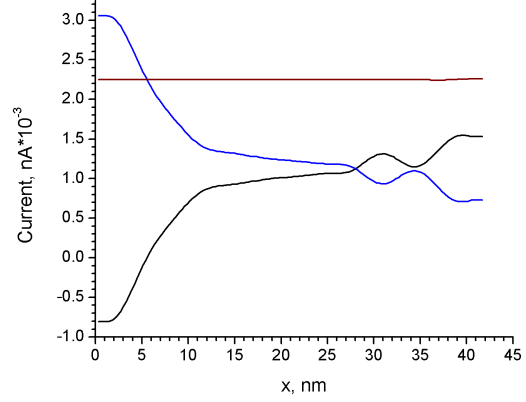


FIG. 8. 2D distribution spectral current for six different photon energies. x-axis units are nm, y-units are eV. Colormap units correspond to nA/eV

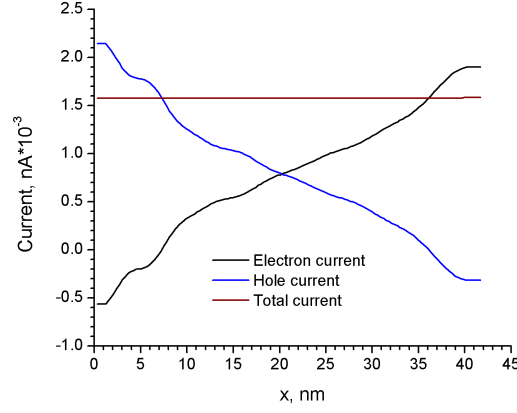
the diode length. These features can be explained by the local generation-recombination rates. Eq.(IV.1) is basically microscopic analog of the macroscopic balance equation¹⁵. Left



(a) $E_\lambda = 1.64$ eV



(b) $E_\lambda = 1.76$ eV



(c) $E_\lambda = 2.00$ eV

FIG. 9. Spatial distribution of hole and electron currents at $E_\lambda = 1.64$ eV, $E_\lambda = 1.76$ eV, $E_\lambda = 2.00$ eV

hand side represents divergence of the particle current(electron) , in our case it is just photo-current due to ballistic photo-extracted carriers. Right hand side is the energy and volume integrated local generation recombination rates. It can be rewritten in the form of Eq's. (IV.2) and (IV.3). Now physical origin of these terms becomes clear. By looking at r.h.s of the Eq.(IV.3) one can see two terms. First one corresponds to the total inscattering rate(generation) at that energy, whereas second term gives total outscattering(recombination) rate at that energy. One should note that by using r.h.s. of the equation (IV.1), and treating particularly first term as inscattering and second as outscattering term may lead to nonphys-

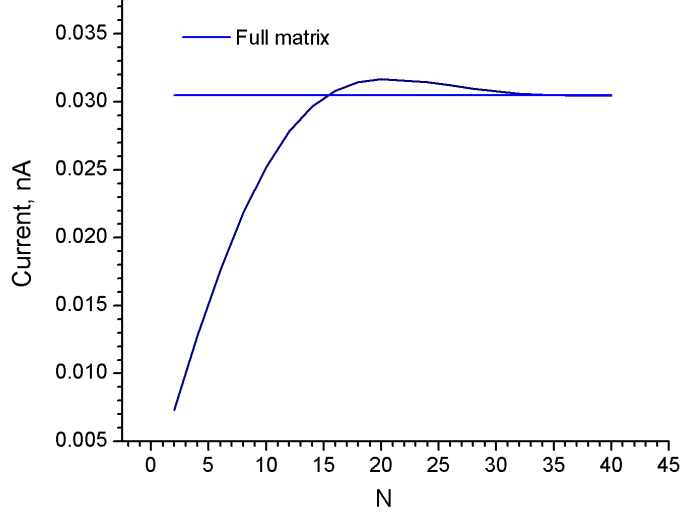


FIG. 10. Current vs. number of Off-diagonals at $E_\lambda = 1.5\text{eV}$ at zero bias for p-i-n structure at $I = 130\text{ W/cm}^2$. Blue line corresponds to full matrix $N = 139$

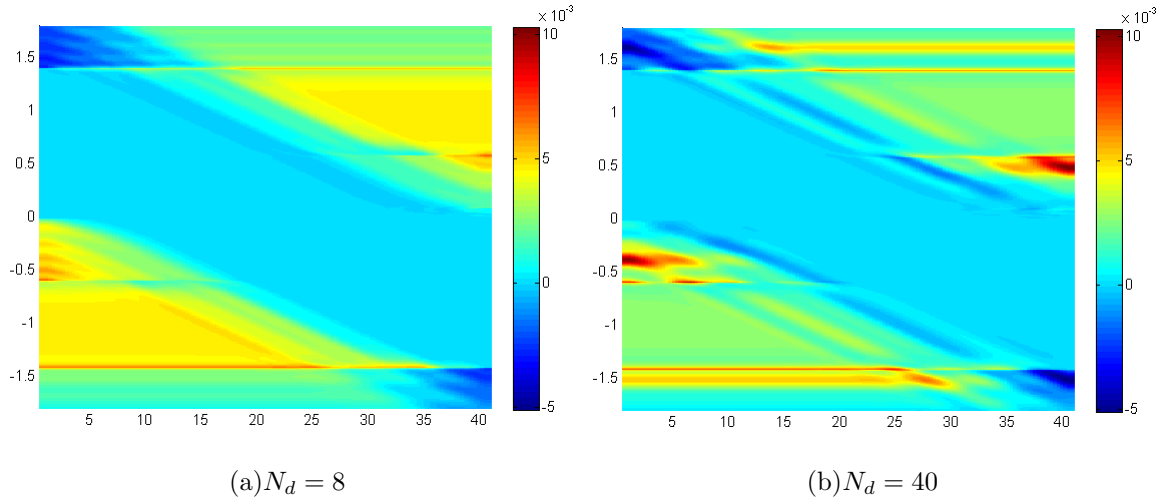


FIG. 11. Effect of number of off-diagonals on the 2D current. a) $N_d = 8$ b) $N_d = 40$, which is approaching full matrix rank

ical features in the local recombination-generation spectra such as appearance of negative inscattering. Although, physical origin of this phenomena is unclear, but we believe it is due to a fact that coherence length in our case is infinite since we are working within ballistic regime. Including non-radiative phase-breaking mechanisms such as phonon-scattering and

working in the limit where mean-free path is smaller than device region should remove this problem.

$$\nabla \cdot \mathbf{J}_{ph} = \frac{1}{V\pi\hbar} \int d^3r \int d^3r' \int dE \{ \Sigma_{e-ph}^<(r, r', E) G^>(r', r, E) - \Sigma_{e-ph}^>(r, r', E) G^<(r', r, E) \} \quad (\text{IV.1})$$

$$\nabla \cdot \mathbf{J}_{ph} = \frac{1}{V\pi\hbar} \int tr[\Sigma_{e-ph}^<(E) \mathbf{G}^>(E) - \Sigma_{e-ph}^>(E) \mathbf{G}^<(E)] dE = \frac{1}{V\pi} \int tr\{\mathbf{I}\} dE \quad (\text{IV.2})$$

$$\mathbf{I}(E) = \frac{1}{\hbar} tr[\Sigma_{e-ph}^<(E) \mathbf{G}^>(E)] - \frac{1}{\hbar} tr[\Sigma_{e-ph}^>(E) \mathbf{G}^<(E)] \quad (\text{IV.3})$$

One can also see that in the case of $E_\lambda=1.76$ eV in Figure 9(b) divergence of the electron and hole current separately is negligible. This indicates that no photocurrent is being generated in the channel region, which is in agreement with Figure 8(e). By tuning the E_λ one can make the diode channel conducting or contact conducting (regions just below valence band and above conduction band). This is also seen in the profiles of the electron and hole currents at different photon energies.

Finally, we also investigate the effect of the non-locality of the Σ_{e-ph} and it's effect on the current densities. It is important to note that recursive implementation will fail in this case since it only accounts for the first off-diagonal terms. As can be seen in Fig.10, by keeping only 2-off diagonal blocks we have a value of the current which is 2.3% of the total current, which is in agreement with the results of Pourfath et. al.³⁰. In addition to this, we have also computed 2D distribution of current density. It is seen that spatial current oscillations are lost in case of $N_d = 8$ as compared to $N_d = 40$, where one reconstructs original picture. The reason for this is wave-like³⁰ behaviour of the self-energy which gives phase-coherent response in the limit of the $N_d \rightarrow N_{total}$, where N_{total} is 139 in our case. Phase coherence is lost once just few off-diagonals are retained. Although, some^{14,15} works consider that only a portion of the device is being illuminated, in this case it can be shown that self-energies Σ_{e-ph} become only band-diagonal, thus giving possibility of inclusion of smaller number of off-band diagonal blocks.

V. CONCLUSIONS AND OUTLOOK.

We have presented the theoretical framework for the computation the opto-electronic response of the 1D devices in the $\mathbf{k} \cdot \mathbf{p}$ model, with particular emphasis on the GaAs material. Extension of the model from direct bandgap materials to the indirect ones for sub-10 nm 1D systems is straightforward but tedious. Phonon scattering incorporation is straightforward. It is shown that in the phase-coherent limit one observes carrier (e, h) spatial current oscillations. It has also been-shown that local recombination-generation rates may lead to negative components of the current at the leads, which in itself deteriorates the device performance. In addition, it was shown that current can flow in the channel region or near the band edges and not in the channel depending on the incident photon energy. Moreover, local generation-recombination rates can form different spatial patterns which is reflected in the features of the photocurrent. Moreover, generation-recombination rates may experience nonphysical behaviour such as negative in-scattering, but we believe this is due to a fact that we are working in the ballistic regime. Effect of the non-locality of the self energy is crucial to the computation of the photo-response both quantitatively and qualitatively. Even two subband model reveals non-trivial behaviour of the electronic response upon light illumination. Numerical results are in reasonable agreement with recent experimental data taking into account number of modes and dimensions of the device. The future work includes more realistic implementation by incorporating more 1D subbands. Penetrable boundaries, band-mixing effects, 3D intraband scattering reflected in 1D inter-subband scattering within CB or VB manifolds, going beyond dipole approximation and more general recursive implementation with finite number of off-diagonals is underway.

REFERENCES

- ¹A. V. J. Ramanujam, D. Shiri, Materials Express **1**, 105–126 (2011).
- ²A. Verma, A. K. Buin, and M. P. Anantram, J. Appl. Phys. **106**, 113713 (2009).
- ³L. Cao, J. S. White, J.-S. Park, J. A. Schuller, B. M. Clemens, and M. L. Brongersma, Nat. Mater. **8**, 643–647 (2009).
- ⁴R. Agarwal and C. M. Lieber, Appl. Phys. A **85**, 209–215 (2006).

- ⁵S. Thunich, L. Prechtel, D. Spirkoska, G. Abstreiter, A. Fontcuberta i Morral, and A. W. Holleitner, *Appl. Phys. Lett.* **95**, 083111 (2009).
- ⁶I. Zardo, S. Yazji, C. Marini, E. Uccelli, A. F. i Morral, G. Abstreiter, and P. Postorino, *ACS Nano* **6**, 3284–3291 (2012).
- ⁷D. Shiri, A. Verma, C. R. Selvakumar, and M. P. Anantram, *Scientific Reports* **2**, 461 (2012).
- ⁸O. Demichel, M. Heiss, J. Bleuse, H. Mariette, and A. F. i Morral, *Appl. Phys. Lett.* **97**, 201907 (2010).
- ⁹C. C. Chang, C. Y. Chi, M. Yao, N. Huang, C. C. Chen, J. Theiss, A. W. Bushmaker, S. LaLumondiere, T. W. Yeh, M. L. Povinelli, C. Zhou, P. D. Dapkus, and S. B. Cronin, *Nano Lett.* **12**, 4484–4489 (2012).
- ¹⁰M. A. Sk, , M.-F. Ng, L. Huang, and K. H. Lim, *Phys. Chem. Chem. Phys.* **15**, 5927–5935 (2013).
- ¹¹C. Colombo, M. Heiβ, M. Gratzel, and A. F. i Morral, *Appl. Phys. Lett.* **94**, 173108 (2009).
- ¹²B. Witzigmann, R. G. Veprek, S. Steiger, and J. Kupec, *J. Comput. Electron.* **8**, 389–397 (2009).
- ¹³A. I. Fedoseyev, M. Turowski, and M. S. Wartak, *J. Nanoelectron. Optoe.* **2**, 234–256 (2007).
- ¹⁴U. Aeberhard and R. H. Morf, *Phys. Rev. B* **77**, 125343 (2008).
- ¹⁵U. Aeberhard, *Nanoscale. Res. Lett.* **6**, 242 (2011).
- ¹⁶S. Steiger, *Modelling Nano-LEDs*, PhD dissertation, Swiss Federal Institute of Technology Zurich (ETHZ) (2009).
- ¹⁷L. E. Henrickson, *J. Appl. Phys.* **91**, 6273–6281 (2002).
- ¹⁸D. A. Stewart and F. Léonard, *Phys. Rev. Lett.* **93**, 107401 (2004).
- ¹⁹E. Kane, edited by W. Paul, Vol. 1 (North-Holland, Amsterdam, 1982) pp. 193–217.
- ²⁰K. Boujdaria, S. Ridene, S. B. Radhia, O. Zitouni, H. Bouchriha, and G. Fishman, *J. Appl. Phys* **92**, 2586–2592 (2002).
- ²¹M. El kurdi, G. Fishman, S. Sauvage, and P. Boucaud, *Phys. Rev. B* **68**, 165333 (2003).
- ²²S. Ridene, K. Boujdaria, H. Bouchriha, and G. Fishman, *Phys. Rev. B* **64**, 085329 (2001).
- ²³K. Boujdaria and O. Zitouni, *Solid State Commun.* **129**, 205 – 210 (2004).
- ²⁴O. Zitouni, K. Boujdaria, and H. Bouchriha, *Semicond. Sci. Technol.* **20**, 908 (2005).

- ²⁵M. Cardona and F. H. Pollak, Phys. Rev. **142**, 530–543 (1966).
- ²⁶T. B. Bahder, Phys. Rev. B **41**, 11992–12001 (1990).
- ²⁷B. A. Foreman, Phys. Rev. B **56**, R12748–R12751 (1997).
- ²⁸C. R. Pidgeon and R. N. Brown, Phys. Rev. **146**, 575–583 (1966).
- ²⁹M. Shin, J. Appl. Phys **106**, 054505 (2009).
- ³⁰M. Pourfath, O. Baumgartner, and H. Kosina, “On the non-locality of the electron-photon self-energy: Application to carbon nanotube photo-detectors,” in *Numerical Simulation of Optoelectronic Devices, 2008. NUSOD '08. International Conference on* (2008) pp. 99–100.
- ³¹R. Lake and S. Datta, Phys. Rev. B **45**, 6670–6685 (1992).
- ³²R. B. Thompson, K. O. . Rasmussen, and T. Lookman, J. Chem. Phys **120**, 31–34 (2004).
- ³³R. K. Lake and R. R. Pandey, arXiv:cond-mat/0607219v1 (2007).
- ³⁴G. D. Mahan, Phys. Rep. **145**, 251 – 318 (1987).
- ³⁵R. C. B. R. K. Lake, G. Klimeck and D. Jovanovic, J. Appl. Phys. **81**, 7845 (1997).
- ³⁶J.-W. Jiang, J.-S. Wang, and B. Li, J. Appl. Phys. **109**, 014326 (2011).
- ³⁷J.-W. Jiang and J.-S. Wang, J. Appl. Phys. **110**, 124319 (2011).
- ³⁸M. Luisier, A. Schenk, and W. Fichtner, J. Appl. Phys. **100**, 043713 (2006).
- ³⁹J. Wang, E. Polizzi, and M. Lundstrom, J. Appl. Phys. **96**, 2192–2203 (2004).
- ⁴⁰J.-W. Jiang, J.-S. Wang, and B. Li, Phys. Rev. B **80**, 205429 (2009).
- ⁴¹S. Birner, T. Zibold, T. Andlauer, T. Kubis, M. Sabathil, A. Trellakis, and P. Vogl, IEEE Trans. Electron Devices **54**, 2137–2142 (2007).
- ⁴²D. Rideau, M. Feraille, M. Michailat, Y. Niquet, C. Tavernier, and H. Jaouen, Solid State Electron. **53**, 452 – 461 (2009).
- ⁴³B. A. Foreman, Phys. Rev. B **52**, 12241–12259 (1995).
- ⁴⁴M. G. Burt, J. Phys.: Condens.Matter **4**, 6651 (1992).
- ⁴⁵W. Yang and K. Chang, Phys. Rev. B **72**, 233309 (2005).
- ⁴⁶B. A. Foreman, Phys. Rev. B **75**, 235331 (2007).
- ⁴⁷R. G. Veprek, S. Steiger, and B. Witzigmann, Phys. Rev. B **76**, 165320 (2007).
- ⁴⁸K. I. Kolokolov, J. Li, and C. Z. Ning, Phys. Rev. B **68**, 161308 (2003).
- ⁴⁹X. Cartoixa, D. Z.-Y. Ting, and T. C. McGill, J. Appl. Phys. **93**, 3974–3981 (2003).
- ⁵⁰T. Eissfeller and P. Vogl, Phys. Rev. B **84**, 195122 (2011).
- ⁵¹J. Guo, M. A. Alam, and Y. Yoon, Appl. Phys. Lett. **88**, 133111 (2006).
- ⁵²U. Aeberhard, Nanoscale Res. Lett. **6**, 242 (2011).

- ⁵³M. F. Pereira and K. Henneberger, Phys. Rev. B **53**, 16485–16496 (1996).
- ⁵⁴U. Aeberhard, Journal of Computational Electronics **10**, 394–413 (2011).
- ⁵⁵A. Lysov, C. Gutsche, M. Offer, I. Regolin, W. Prost, and F. J. . Tegude, “The optoelectronic performance of axial and radial gaas nanowire pn-diodes,” in *Compound Semiconductor Week (CSW/IPRM), 2011 and 23rd International Conference on Indium Phosphide and Related Materials* (2011) pp. 1–3.
- ⁵⁶U. Aeberhard, Optical and Quantum Electronics **44**, 133–140 (2012).